NOAA Technical Report NWS 30

The NMC Spectral Model

Silver Spring, Md.
May 1982

U. S. DEPARTMENT OF COMMERCE
National Oceanic and Atmospheric Administration
National Weather Service

NOAA TECHNICAL REPORTS

National Weather Service Series

The National Weather Service (NWS) observes and measures atmospheric phenomena; develops and distributes forecasts of weather conditions and warnings of adverse weather; collects and disseminates weather information to meet the needs of the public and specialized users. The NWS develops the national meteorological service system and improves procedures, techniques, and dissemination for weather and hydrologic measurements, and forecasts.

NWS series of NOAA Technical Reports is a continuation of the former series, ESSA Technical Report Weather Bureau (WB).

Reports listed below are available from the National Technical Information Service, U.S. Department of Commerce, Sills Bldg., 5285 Port Royal Road, Springfield, Va. 22161. Prices vary. Order by accession number (given in parentheses).

ESSA Technical Reports

WB 1 Monthly Mean 100-, 50-, 30-, and 10-Millibar Charts January 1964 through December 1965 of the IQSY Period. Staff, Upper Air Branch, National Meteorological Center, February 1967, 7 p, 96 charts. (AD 651 101)

WB 2 Weekly Synoptic Analyses, 5-, 2-, and 0.4-Mb Surfaces for 1964 (based on observations of the Meteorological Rocket Network during the IQSY). Staff, Upper Air Branch, National Meteorological Center, April 1967, 16 p, 160 charts. (AD 652 696)

WB 3 Weekly Synoptic Analyses, 5-, 2-, and 0.4-Mb Surfaces for 1965 (based on observations of the Meteorological Rocket Network during the IQSY). Staff, Upper Air Branch, National Meteorological Center, August 1967, 173 p. (AD 662 053)

WB 4 The March-May 1965 Floods in the Upper Mississippi, Missouri, and Red River of the North Basins. J. L. H. Paulhus and E. R. Nelson, Office of Hydrology, August 1967, 100 p.

WB 5 Climatological Probabilities of Precipitation for the Conterminous United States. Donald L. Jorgensen, Techniques Development Laboratory, December 1967, 60 p.

WB 6 Climatology of Atlantic Tropical Storms and Hurricanes. M. A. Alaka, Techniques Development Laboratory, May 1968, 18 p.

WB 7 Frequency and Areal Distributions of Tropical Storm Rainfall in the United States Coastal Region on the Gulf of Mexico. Hugo V. Goodyear, Office of Hydrology, July 1968, 33 p.

WB 8 Critical Fire Weather Patterns in the Conterminous United States. Mark J. Schroeder, Weather Bureau, January 1969, 31 p.

WB 9 Weekly Synoptic Analyses, 5-, 2-, and 0.4-Mb Surfaces for 1966 (based on meteorological rocketsonde and high-level rawinsonde observations). Staff, Upper Air Branch, National Meteorological Center, January 1969, 169 p.

WB 10 Hemispheric Teleconnections of Mean Circulation Anomalies at 700 Millibars. James F. O'Connor, National Meteorological Center, February 1969, 103 p.

WB 11 Monthly Mean 100-, 50-, 30-, and 10-Millibar Charts and Standard Deviation Maps, 1966-1967. Staff, Upper Air Branch, National Meteorological Center, April 1969, 124 p.

WB 12 Weekly Synoptic Analyses, 5-, 2-, and 0.4-Millibar Surfaces for 1967. Staff, Upper Air Branch, National Meteorological Center, January 1970, 169 p.

NOAA Technical Reports

NWS 13 The March-April 1969 Snowmelt Floods in the Red River of the North, Upper Mississippi, and Missouri Basins. Joseph L. H. Paulhus, Office of Hydrology, October 1970, 92 p. (COM-71-50269)

NWS 14 Weekly Synoptic Analyses, 5-, 2-, and 0.4-Millibar Surfaces for 1968. Staff, Upper Air Branch, National Meteorological Center, May 1971, 169 p. (COM-71-50383)

NWS 15 Some Climatological Characteristics of Hurricanes and Tropical Storms, Gulf and East Coasts of the United States. Francis P. Ho, Richard W. Schwerdt, and Hugo V. Goodyear, May 1975, 87 p. (COM-75-11088)

(Continued on inside back cover)

NOAA Technical Report NWS 30

The NMC Spectral Model

Joseph G. Sela

Silver Spring, Md.
May 1982

U. S. DEPARTMENT OF COMMERCE
Malcolm Baldrige, Secretary

National Oceanic and Atmospheric Administration
John V. Byrne, Administrator

National Weather Service
Richard E. Hallgren, Director

TABLE OF CONTENTS

		Page
1.	Introduction	1
2.	Model Description	3
3.	The Prediction Equations in Spectral Form	11
4.	Normal Modes Initialization	13
5.	Acknowledgment	18
6.	References	19
7.	Appendix A, The Arakawa Vertical Finite Differencing Scheme	21
8.	Appendix B, Basic Spectral Concepts	24

TABLES

1.	Gravity Wave Statistics	29
2.	Gaussian Latitudes and Weights for J=30	30

LIST OF FIGURES

1.	Vertical Layer Structure	31
2.	Surface Pressure Trace With and Without Initialization	32
3.	RMS Divergence Trace With and Without Initialization	33
4.	The Gaussian Grid	34
5.	The Rhomboidal Truncation	35
6.	S1 Scores Statistics	36

THE NMC SPECTRAL MODEL

Joseph G. Sela
National Weather Service, National Meteorological Center, NOAA
Camp Springs, MD

ABSTRACT. A model with spectral representation in the horizontal and Arakawa quadratic conserving finite differencing in the vertical is described. The model includes a moisture cycle consisting of large-scale condensation processes, as well as a convective parameterization. Interactions with the underlying oceans include evaporation and sensible heating. Orography and surface friction are modeled and a semi-implicit time integration is employed. Machenhauer's normal modes initialization method is applied.

1. INTRODUCTION

This report is a documentation of the Spectral Model currently in operation at NMC in the Data Assimilation Final Cycle and the Large Scale forecast cycle. The report is divided into four sections, the first of which is this introduction.

In section 2 the model formulation is described and the equations governing the history variables are derived. Appendix A is included for reference to the Arakawa vertical finite differencing scheme used in the model's formulation.

Section 3 deals with spectral aspects of the model's equations. The reader may wish to refer to Appendix B for additional details concerning the transform technique as well as some information regarding the Hough functions to spherical harmonic conversion.

Section 4 describes the implementation of the Machenhauer nonlinear normal modes initialization as presently applied to the sigma input data. A more complete exposition of initialization problems and techniques can be found in Ballish (1980).

The development of a Spectral Model at NMC evolved from Numerical Weather Prediction experience using the Seven Layer PE grid point model, Shuman and Hovermale (1968); the Limited Area Fine Mesh model, Gerrity (1977); and experiments in spectral techniques by Bourke (1974).

During the initial model development stages the question of the spectral resolution needed for operational quality forecasts was not resolved. To permit flexibility in addressing this question the model was designed and coded in very general terms. Generalized codes were especially useful in subsequent experiments regarding an operational global medium range forecast system and in transporting the model to other computer installations possessing different computing capabilities.

The results of numerous resolution experiments led to two basic versions of 24 and 30 waves in a rhomboidal expansion, depicted in figure 5, now used at NMC. The Spectral Model can be executed with an arbitrary resolution, but the above two are better optimized. The rhomboidal truncation was chosen to permit higher meridional resolution of larger scale disturbances. It was recognized that the rotational invariance property found in a triangular truncation would be lost, but this property is never invoked in the formulation or computer implementation.

The vertical resolution now in use consists of twelve layers for the 84-hr forecast period, diminishing to six layers for the extended 84-hr to 192-hr range. This choice is a compromise between an attempt to employ a global system and operational schedules.

The vertical coordinate of the model is $\sigma = 1 - P/P_*$, defined by Phillips (1959), with a specification of layer locations described by Brown (1974) and Phillips (1975). Finite differencing in the vertical is applied. The choice of a quadratic conserving scheme, Arakawa and Mintz (1974), was motivated by the belief that the adiabatic model's equations should reproduce as many characteristics of the continuous equations as possible, an attitude not shared by all modelers. A small fringe benefit resulting from this choice arises during the preliminary coding stages of the model by diagnosing programming errors through the monitoring of conservative quantities.

The physical effects included in the model are influences of orography, position-dependent surface friction, and subscale horizontal dissipation parameterized by diffusion. The moisture cycle is based on a mixing ratio formulation with large scale precipitation as well as Kuo-type convection, Kuo (1965), and evaporation from the oceans. Sensible heating from underlying water is also included.

The time integration is semi-implicit, Robert (1969), with a moderate time filter. During the initial experiments the semi-implicit backward time integration was advantageously employed to suppress high frequency gravity-waves noise. With the introduction of the normal modes initialization, Ballish (1980), the time integration was changed to semi-implicit centered.

The Spectral Model was implemented operationally at NMC in 1980. The Final Data Assimilation Cycle began using a spectral "guess" in June, and the Large Scale forecast cycle became spectral in August. Each implementation was preceded by extensive testing and evaluation. Results of the Final Cycle tests can be found in a documentation by Kistler and Parrish (1981). The comparisons with the 7L PE were documented by Stackpole (1980). An evaluation of the Medium-Range 5-10 days Forecast System was documented by Hughes (1981).

It was demonstrated in all applications that the spectral method has superior computational and gravitational noise control, is particularly advantageous in short forecasts used in a 6-hr assimilation cycle, and produces forecasts similar to the 7L PE in the middle and lower troposphere. At the jet stream level the spectral forecasts appear to possess the ability to maintain intense speeds throughout the forecast period.

The precipitation forecasts from the spectral model are however inferior to the 7L PE and work to improve their spread and accumulation amounts continues. (The primary tools for precipitation events for the U.S. area are the Limited Fine Mesh and the Movable Fine Mesh models).

A summary of performance statistics and comparison with the LFM model was prepared by the Systems Evaluation Branch and is displayed in figure 6. This figure displays S1 scores of 500 mb and MSL pressure for 12 hr, 24 hr, 36 hr, and 48 hr. The graphs on the right display the annual means for the years 1976 through 1980. The Spectral Model affects the annual mean of 1980 only.

2. MODEL DESCRIPTION

Some of the variables appearing in the description are listed below:

$\vec{v}_k$ = horizontal velocity at layer k

$\hat{\dot{\sigma}}_k = \frac{d\sigma}{dt}$ at interface (level) k

$\sigma = 1 - p/p_*$, vertical coordinate

p = pressure

p_* = surface pressure

Φ_k = geopotential at layer k

T_k = temperature at layer k

f = Coriolis parameter

$\vec{k}$ = vertical unit vector

∇ = Del operator

θ = potential temperature

$\kappa = R/c_v$

c_p = specific heat of air at constant pressure

c_v = specific heat of air at constant volume

R = air gas constant

$(\hat{\ }) = (\ )$ at layer k (k = 1 corresponds to surface)

$c_j = \vec{v}_j \cdot \nabla \ln p_*$

$(\bar{\ }) = \sum_{j=1}^{K} \Delta_j (\ )_j$ = finite difference vertical integral

Δ_j = layer sigma thickness (see figure 1)

K = number of model layers (= Levels - 1)

λ = longitude; ϕ = latitude

a = radius of earth

$( )_n^{\ell}$ = spectral coefficient (only when both indices are letters)

ψ = stream function

χ = velocity potential

$D = \nabla \cdot \vec{V}$

$(\underline{\ })$ = square matrix

Ω = angular velocity of the earth

Considering figure 1 for the location of layer and interface variables, the formulation of the quadratic conserving vertical finite-differencing scheme results in the following:

Momentum equation

$$\frac{\partial \vec{v}_k}{\partial t} + (\vec{v} \cdot \nabla)\vec{v}_k + \frac{1}{2\Delta_k}\left[\dot{\hat{\sigma}}_{k+1}(\vec{v}_{k+1} - \vec{v}_k) + \dot{\hat{\sigma}}_k(\vec{v}_k - \vec{v}_{k-1})\right] = - \nabla\Phi_k - RT_k\nabla \ell n\, p_* - f\,\vec{k} \times \vec{v}_k \,. \tag{1}$$

Thermodynamic equation

$$\frac{\partial T_k}{\partial t} + \vec{v}_k \cdot \nabla T_k + \frac{1}{2\Delta_k}\left[\dot{\hat{\sigma}}_{k+1}\left(\frac{\pi_k}{\pi_{k+1}} T_{k+1} - T_k\right) + \dot{\hat{\sigma}}_k\left(T_k - \frac{\pi_k}{\pi_{k-1}} T_{k-1}\right)\right] = \kappa T_k\left(\frac{\partial}{\partial t} + v_k \cdot \nabla\right) \ell n\, p_* . \tag{2}$$

$$\frac{\partial}{\partial t} \ell n\, p_* = - \overline{c} - \overline{D} \,. \tag{3}$$

$\dot{\hat{\sigma}}_k$ is diagnosed from

$$\dot{\hat{\sigma}}_{k+1} = \hat{\sigma}_{k+1}(\overline{D} + \overline{c}) - \sum_{j=1}^{k} \Delta_j (D_j + c_j) \tag{4}$$

subject to boundary conditions

$$\dot{\hat{\sigma}}_1 = \dot{\hat{\sigma}}_{K+1} = 0.$$

The geopotential at layer k, Φ_k, is obtained from a simultaneous system of equations specified by the similarity of the continuous and discretized equations, see Appendix A. These are

$$\Phi_{k-1} - \Phi_k = \frac{c_p}{2}\left[T_{k-1}\left(\frac{\pi_k}{\pi_{k-1}} - 1\right) + T_k\left(1 - \frac{\pi_{k-1}}{\pi_k}\right)\right] \qquad k = 2\ldots K \tag{5}$$

and

$$\sum_{j=1}^{K} \Delta_j \Phi_j = \hat{\Phi}_1 + R \sum_{j=1}^{K} \Delta_j T_j \,, \tag{6}$$

where Φ_1 is the known and fixed surface geopotential. With $(\tilde{\ })$ denoting a transpose, these K equations may be written as

$$\underline{H}\tilde{\Phi} = \underline{B}\tilde{T} + \tilde{\hat{\Phi}} \quad \text{or} \quad \tilde{\Phi} = \underline{A}\tilde{T} + \underline{H}^{-1}\tilde{\hat{\Phi}} \tag{7}$$

in which $\underline{H}$, $\underline{B}$, and $\underline{A}$ are geographically constant square coefficient matrices, and

$$\Phi = \left(\Phi_1 \cdots \Phi_k\right), \quad T = \left(T_1 \cdots T_k\right), \quad \hat{\Phi} = \left(\,o \cdots o\, \hat{\Phi}_1\right). \tag{8}$$

According to Arakawa, we let level values be related to layer values by prescribing

$$\hat{\theta} = \tfrac{1}{2}\left(\theta_k + \theta_{k-1}\right) \tag{9}$$

to conserve θ^2 and similarly for other variables. Following Brown (1974) and Phillips (1975), we set

$$\pi_k = \frac{\hat{p}_k^{1+\kappa} - \hat{p}_{k+1}^{1+\kappa}}{(1+\kappa)\left(\hat{p}_k - \hat{p}_{k+1}\right)} \sim \frac{1}{(1+\kappa)} \frac{d}{dp} p^{(1+\kappa)}. \tag{10}$$

This definition of the layer pressure ensures that the total enthalpy in each layer at each geographic location equals that in the atmosphere if the latter has $\partial\theta/\partial\sigma = 0$ in each layer.

The differentiated equations are derived by operating on the momentum equation with $\nabla_\sigma \cdot$ and $\vec{k}\cdot\nabla_\sigma \times$.

Defining

$$D_k = \nabla_\sigma \cdot \vec{v}_k \qquad \zeta_k = \vec{k}\cdot\nabla_\sigma \times \vec{v}_k$$

$$\eta_k = \zeta_k + f \qquad E_k = \tfrac{1}{2}(v_k \cdot v_k) \tag{11}$$

we may write for k = 1...K

$$\frac{\partial \eta_k}{\partial t} = -\frac{1}{a\cos^2\phi}\left(\frac{\partial A_k}{\partial \lambda} + \cos\phi \frac{\partial B_k}{\partial \phi}\right) \tag{12}$$

$$\frac{\partial D_k}{\partial t} = \frac{1}{a \cos^2\phi}\left(\frac{\partial B_k}{\partial \lambda} - \cos\phi \frac{\partial A_k}{\partial \phi}\right) - \nabla^2\left(\phi_k + RT_{o,k} \ell n\, p_* + E_k\right) . \quad (13)$$

These are the vorticity and divergence equations as derived by Bourke (1974). Note, however, that equation (12) describes the absolute vorticity. In these equations,

$$A_k = \eta_k U_k + RT_k' \frac{\cos\phi}{a} \frac{\partial\, \ell n\, p_*}{\partial \phi} + \frac{1}{2\Delta_k}\left[\hat{\dot{\sigma}}_{k+1}\left(V_{k+1} - V_k\right) + \hat{\dot{\sigma}}_k\left(V_k - V_{k-1}\right)\right] \quad (14)$$

$$B_k = \eta_k V_k - RT_k' \frac{1}{a} \frac{\partial\, \ell n\, p_*}{\partial \lambda} - \frac{1}{2\Delta_k}\left[\hat{\dot{\sigma}}_{k+1}\left(U_{k+1} - U_k\right) + \hat{\dot{\sigma}}\left(U_k - U_{k-1}\right)\right] \quad (15)$$

and the pseudo velocity is defined by

$$(U_k, V_k) = \cos\phi(u_k, v_k) . \quad (16)$$

$T_k = T_{o,k} + T_k'$ where $T_{o,k}$ is some constant temperature at layer k.

The thermodynamic equation is now written in a form suitable for a semi-implicit integration, Robert (1969). The objective is to separate the linear contribution of divergence terms from the rest of the terms appearing in the thermodynamic equation. This is achieved by substituting $\hat{\dot{\sigma}}$ from equation (4) into equation (2). We now define the following notation:

$$\pi_1^1 = \frac{\pi_1}{\pi_2} \ldots \pi_k^1 = \frac{\pi_k}{\pi_{k+1}} \ldots \pi_K^1 = 0$$

$$\pi_1^2 = 0 \quad \ldots \pi_k^2 = \frac{\pi_k}{\pi_{k-1}} \ldots \pi_K^2 = \frac{\pi_K}{\pi_{K-1}} \quad (17)$$

$$H_1^1 = \pi_1^1 T_2^0 - T_1^0 \ldots H_k^1 = \pi_k^1 T_{k+1}^0 - T_k^0 \ldots H_K^1 = 0$$

$$H_1^2 = 0 \quad \ldots H_k^2 = T_k^0 - \pi_k^2 T_{k-1}^0 \ldots H_K^2 = T_K^0 - \pi_K^2 T_{K-1}^0 .$$

π_k^1 and π_k^2 are fixed in time and space being functions only of k. H_k^1 and H_k^2 may vary with time, however. Using the above relations, equation (2) may be written in the form

$$\frac{\partial T_k}{\partial t} = S_k + \sum_{j=1}^{K} b_{k,j} D_j , \quad (18)$$

where

$$S_k = -\vec{v}_k \cdot \nabla T_k' - \kappa T_k' \overline{D} + \kappa\left(T_k^0 + T_k'\right)\left(c_k - \overline{c}\right)$$

$$- \frac{1}{2\Delta_K}\left[\hat{\sigma}_{k+1}\left(\pi_k^1 T'_{k+1} - T_k'\right) + \hat{\sigma}_k\left(T_k' - \pi_k^2 T'_{k-1}\right)\right. \tag{19}$$

$$\left. + \left(\hat{\sigma}_{k+1}\overline{c} - \sum_{j=1}^{k} \Delta_j c_j\right) H_k^1 + \left(\hat{\sigma}_k \overline{c} - \sum_{j=1}^{k-1} \Delta_j c_j\right) H_k^2\right].$$

The matrix $b_{k,j}$ comes from terms in (2) which depend on the layer divergences D_k:

$$\sum_{j=1}^{K} b_{k,j} D_j = \frac{1}{2\Delta_k}\left[\left(H_k^1 + H_k^2\right) \sum_{j=1}^{k} \Delta_j D_j - H_k^2 \Delta_k D_k\right] \tag{20}$$

$$- \left[\kappa T_k^0 + \frac{1}{2\Delta_k}\left(\hat{\sigma}_{k+1} H_k^1 + \hat{\sigma}_k H_k^2\right)\right] \sum_{j=1}^{K} \Delta_j D_j \ .$$

It is pointed out that this is not the only way to implement a semi-implicit scheme. Another separation can be affected by linearizing the thermodynamic equation's potential to kinetic energy conversion term only.

The continuity equation (3), the divergence equation (13), and the thermodynamic equation (18) can now be treated semi-implicitly.

At this point, the evaluation of the linear terms should be specified. Let $\tau-1$, τ, $\tau+1$ be three consecutive time steps and consider equation (18) in finite difference form. We may write

$$\tilde{T}(\tau+1) = \tilde{T}(\tau-1) + 2\Delta t\left[\tilde{S}(\tau) + \underline{B}\left(\alpha\tilde{D}(\tau+1) + (1-\alpha)\tilde{D}(\tau-1)\right)\right]. \tag{21}$$

For $\alpha = 1/2$, we obtain the conventional semi-implicit scheme. Integrations with this value of α were found to be rather noisy. Efforts to suppress initial data imbalances using initially strong horizontal diffusion (Bourke, 1974) resulted in smoother "barographs." Setting $\alpha = 1$, we obtain the backward semi-implicit scheme and integrations with this choice of α are much smoother. The application of Machenhauer's nonlinear normal modes initialization provides an excellent method of suppressing the high frequency noise encountered with $\alpha = \frac{1}{2}$ and was employed in a 10-case evaluation. The details of this method as implemented in the present model are presented in section 4. We complete the discussion of the time integration by presenting the time filter, Robert (1965), applied to all variables. It is of the form

$$F^*(\tau) = \beta F(\tau) + \left(F(\tau-1) + F(\tau+1)\right)(1-\beta)/2,$$

where $\beta = 0.92$ and $F(\tau+1)$ is the just predicted value of F. $F^*(\tau)$ is the $F(\tau-1)$ for the next time step. Since the codes are core-contained, this implementation is straightforward.

We can now turn to the various physical effects incorporated into the model.

The influence of orography is modeled spectrally and will be presented in the section treating the spectral form of the model's equations. However, the gridded field of mountains used by NMC's operations is passed through a nine-point filter twice to remove excessive oceanic irregularities when expressed spectrally. Using the raw gridded fields results in somewhat inferior forecasts.

Lower boundary friction is simulated using Bourke's (1974) formulation but with a geographically variable drag coefficient C_d, Cressman (1960). This horizontal field resembles the orography distribution with values of 1.29×10^{-3} over water and reaching 8.5×10^{-3} MTS Units over the Rocky and Tibet mountains.

Sensible heat transfer from the underlying surface is allowed only over water regions. The rate of heating of the lowest model layer is parameterized by the term on the right in the thermodynamic equation:

$$\frac{\partial T(1)}{\partial t}\ldots = \ldots + (c_d + 7.10^{-5}|\vec{v}|)\,|\vec{v}|(\theta_s - \theta(1))/h, \qquad (22)$$

where h is the thickness of the bottom layer, $|\vec{v}|$ and θ (1) are the wind speed and potential temperature in that layer, and θ_s is the potential temperature at the surface. The effect is seen to be selective, higher by a factor of 2 to 3 under high wind conditions, Roll (1965). No sensible heat from the continents is allowed at this stage.

Finally, subscale dissipation is parameterized by a horizontal diffusion term of the form $k\nabla^4 F$, where F is any of the prognostic variables except the surface pressure. The value of $k = 6 \times 10^{15}$ was found satisfactory. It should be mentioned that the full model with diabatic effects will be unstable in the absence of diffusion. The numerical implementation of this effect is performed as a modification to the nonlinear tendencies using lagged (τ-1) values of the appropriate variables. No vertical diffusion is applied currently.

To complete the prognostic system, an equation for the moisture mixing ratio Q is required. If we designate source and sink terms by S_r and S_i we may write

$$\frac{dQ}{dt} = S_r - S_i \ , \quad \text{or}$$

$$\frac{\partial Q_k}{\partial t} + \vec{V}_k \cdot \nabla Q_k + \frac{1}{2\Delta_k}[\dot{\hat{\sigma}}_{k+1}(Q_{k+1} - Q_k) + \dot{\hat{\sigma}}_k(Q_k - Q_{k-1})] = S_r - S_i \cdot \qquad (23)$$

In the last equation, the vertical finite differencing used in the other model equations was introduced.

The main source of moisture arises from evaporation at the lower boundary. To parameterize this effect, we again adopt a formulation that permits the process to be wind-speed selective. In this approach

$$S_r = \frac{(c_d + 7.10^{-5}|\vec{v}|)|\vec{v}|}{h} (Q_s - Q(1)) \qquad (24)$$

where Q_s is the mixing ratio corresponding to the sea surface temperature specified by monthly normals. No evaporation from moist ground is allowed.

Moisture sinks result from convective and large-scale condensation accumulated every time step at each point of the computational grid. This grid arises in the implementation of the transform method and appears to be suitable for the inclusion of physical effects that do not lend themselves to simple spectral techniques. The transform method is described in Appendix B.

The integration of the moisture equation proceeds in several steps. A preliminary forecast is made in tandem with the other model variables. The new values of mixing ratio and temperature are first subjected to a Kuo-type convection process followed by a large-scale condensation algorithm. Next, the modified temperature field is adjusted whenever dry superadiabatic conditions are encountered. Under such unstable conditions, the temperature field undergoes a dry convective adjustment and the moisture content of a column is redistributed in the vertical to reflect the adjusted temperature profile. The forecast step is completed by incorporating the adjusted fields in the time filter.

The Kuo-type convection is an adaptation of Phillips' (1979) treatment of organized moist convective processes in his Nested Grid Model. This process is invoked in the presence of large moisture convergence accompanied by a moist unstable lapse rate under moderately high relative humidity conditions.

The highlights of the method consist of computing moisture convergence in the first four bottom layers of each column. If the computed amounts exceed a specified threshold (10^{-7} cb/sec in the 30-wave 12-layer version), a moist adiabat is computed for the column, assuming that the first layer is saturated and using the preliminary pressure and temperature prediction. An unstable region is then defined from the bottom layer to the first layer which is warmer than a moist adiabatically lifted parcel. If such an unstable column is found, the following sums are computed from layer 2 to the top of the unstable part of the column

$$Q_1 = \frac{P_*}{g} \Sigma(q_{cld} - q_k)\Delta\sigma_k$$

$$Q_2 = \frac{c_p P_*}{Lg} \Sigma(T_{cld} - T_k)\Delta\sigma_k$$

and

$$Q_{eff} = \text{Water}/(Q_1 + Q_2)$$

$$DTKUO_k = Q_{eff}(T_{cld} - T_k)$$

$$DQKUO_k = Q_{eff}(q_{cld} - q_k).$$

The above are equations (4.3) through (4.7) in Phillips (1979). The term for water in the expression for Q_{eff} is the moisture convergence in the unstable column, q_{cld} and T_{cld} are the lifted parcel values of saturation humidity and temperature at layer k, and $L = 2.5 \times 10^6$ kJ/ton is the latent heat. $DTKUO_k$, when positive, represents the latent heat release of convective precipitation and is added to the preliminary temperature forecast. $DQKUO_k$ represents the revised value of the change in specific humidity and is therefore added to the value at the previous time step. To prevent convective precipitation when the environment is unstable but relatively dry, condensed falling water is allowed to evaporate into lower layers.

The large-scale precipitation algorithm compares the forecast value of Q with a modified saturation value at forecast temperatures and pressures in the sigma layers. In the event of supersaturation, the excess moisture is allowed to condense and re-evaporate as it moves through lower unsaturated layers. The predicted temperature field is adjusted in accordance with the amount of latent heat released in the process, and condensed moisture penetrating the bottom layer is accumulated.

The modified saturation value is based on a specification proposed by Hirano (personal communication), and used by Stackpole (Stackpole, 1978) in the Nine-Layer Global Model. The modification consists of diminishing the analytical saturation mixing ratio, depending on pressure and temperature alone, by a reduction factor S_p depending on the layer's elevation. Thus precipitation can be formed in a layer with relative humidity less than 100 percent. The reduction factor begins with a value of 1.0 at the lowest layer, and diminishes to 0.8 at the top moist layer. In the second and third layers, the factor is a function of the temperature at the bottom layer according to:

$$S_p = 0.8 \qquad T \leq -12.5°C.$$

$$S_p = 0.8 - 0.005(0.015\ T^2 - 0.734\ T - 11.6) \qquad -12.5 \leq T \leq 18.5.$$

$$S_p = 0.9 \qquad T > 18.5.$$

This highly empirical specification resulted in improved precipitation forecasts compared to those obtained with a constant saturation criterion.

3. THE PREDICTION EQUATIONS IN SPECTRAL FORM

In the following, all prognostic variables will be assumed to be represented by spherical harmonic series of the form

$$D = \sum_{\ell=-J}^{J} \sum_{n=|\ell|}^{|\ell|+J} D_n^\ell \, p_n^\ell(\sin\phi) e^{i\ell\lambda}, \tag{25}$$

where D_n^ℓ are the complex expansion coefficients, P_n^ℓ are Legendre polynomials of the first kind, and ℓ is the zonal wave number. The truncation is rhomboidal, and there are $(J+1)^2$ such coefficients for each of the prognostic fields at each layer.

The diagnostic variables required at each time step are the geopotential, computed spectrally from the hydrostatic relation equation (7), and the spectral temperature, as well as the velocity obtained spectrally from the divergence and vorticity. It is noted that the pseudo-velocity must be truncated in the manner

$$(U,V) = (u,v)\cos\phi = \sum_{\ell=-J}^{J} \sum_{n=|\ell|}^{|\ell|+J+1} (U_n^\ell, V_n^\ell) p_n^\ell(\sin\phi) e^{i\ell\lambda} \tag{26}$$

to be compatible with the assumed truncation in the vorticity and divergence series (Eliasen et al., 1970).

The differential prediction equations in spectral form have been treated in detail by Bourke (1974). The procedure (see Appendix B) is to isolate a particular tendency component of any of the history variables' coefficients by multiplying the relevant equation by the complex conjugate of the desired component, performing a surface integral on the sphere, and using the orthonormality relations of the surface harmonics. The longitudinal dependence is easily integrated out, while a meridional integration by parts in conjunction with the application of the Legendre polynomials' boundary values at the poles results in the following equations. With layer subscripts now understood and A_ℓ and B_ℓ representing Fourier coefficients of A and B, we have

$$\frac{\partial}{\partial t} \eta_n^\ell = \int_{-\frac{\pi}{2}}^{\frac{\pi}{2}} \frac{1}{a\cos^2\phi} \left(-i\ell A_\ell p_n^\ell + B_\ell \cos\phi \frac{d}{d\phi} p_n^\ell \right) \cos\phi \, d\phi, \tag{27}$$

$$\frac{\partial}{\partial t} D_n^\ell = \int_{-\frac{\pi}{2}}^{\frac{\pi}{2}} \frac{1}{a\cos^2\phi} \left(i\ell B_\ell p_n^\ell + A_\ell \cos\phi \frac{d}{d\phi} p_n^\ell \right) \cos\phi \, d\phi + \frac{n(n+1)}{a^2} \left(\phi_n^\ell + E_n^\ell + RT_o q_n^\ell \right), \tag{28}$$

$$\frac{\partial}{\partial T} T_n^{\ell}(k) = S_n^{\ell}(k) + \sum_{j=1}^{K} b_{k,j} D_n^{\ell}(j), \tag{29}$$

$$\frac{\partial}{\partial t} q_n^{\ell} = - \overline{c_n^{\ell}} - \overline{D_n^{\ell}}. \tag{30}$$

In the above, equation (27) is the spectral form of the vorticity equation (12), equation (28) is derived from the divergence equation (13), equation (29) comes from the thermodynamic equation (18), and equation (30) is the spectral form of equation (3) where q represents the logarithm of the surface pressure. The above four equations are the analogs of Bourke's (1974) equations (28), (29), (30), and (31), respectively. The moisture equation (23) is also spectrally represented as

$$\frac{\partial Q_n^{\ell}}{\partial t} = G_n^{\ell}, \tag{31}$$

where G_n are the spectral components of the mixing ratio tendency. Equations (27) and (31) are solved explicitly using centered time differencing.

The spectral equations appropriate for semi-implicit implementation will now be given. Defining the vectors

$$\begin{aligned} \Delta &= -\left(\Delta_1,\ldots,\Delta_K\right) & S &= \left(S_n^{\ell}(1),\ldots,S_n^{\ell}(K)\right) \\ x &= \left(x_n^{\ell}(1)\ldots\ x_n^{\ell}(K)\right), & D &= \left(D_n^{\ell}(1)\ \ldots\ D_n^{\ell}(K)\right) \\ T &= \left(T_n^{\ell}(1)\ldots\ T_n^{\ell}(K)\right), & T_o &= \left(T_o(1)\ \ldots\ T_o(K)\right), \end{aligned} \tag{32}$$

we write, paralleling Bourke (1974)

$$x_n^{\ell}(k) = \int_{-\frac{\pi}{2}}^{\frac{\pi}{2}} \frac{1}{a\cos^2\phi}\left\{ i\,\ell\, B_{\ell}(k) P_n^{\ell} + A_{\ell}(k)\cos\phi\,\frac{dp_n^{\ell}}{d\phi}\right\}\cos\phi\ d\phi + \frac{n(n+1)}{a^2} E_n^{\ell} + \frac{n(n+1)}{a^2}\left(H^{-1}\,\tilde{\hat{\Phi}}\right)_k, \tag{33}$$

where the last term represents the effects of orography, and

$$\frac{\partial \tilde{D}}{\partial t} = \tilde{x} + \frac{n(n+1)}{a^2} \underline{A}\tilde{T} + R\, q_n^{\ell}\, \tilde{T}_o \Big), \tag{34}$$

$$\frac{\partial \tilde{T}}{\partial t} = \tilde{S} + \underline{B}\, \tilde{D}, \tag{35}$$

$$\frac{\partial q_n^{\ell}}{\partial t} = - c_n^{\ell} + \Delta\, \tilde{D}. \tag{36}$$

Equations (34), (35), and (36) are finite differenced in time as described in equation (21) with $\alpha = \frac{1}{2}$, and there are $(J+1)^2$ such systems of equations.

4. NORMAL MODES INITIALIZATION

This section describes the application of the normal modes initialization technique developed by Machenhauer (1977). The original implementation of the method in the global model was done by Ballish as part of his doctoral thesis. The hemispheric code was implemented by the writer after the benefits of the method were experimentally established by Ballish. The derivation below departs from Ballish's work only in the method of arriving at the spectral linearized model and some aspects of the matrix computations. The removal of the ambiguity in initializing the so-called composite variable is due to Ballish and constitutes a definite contribution.

A normal mode of the model's linear version is a solution of ζ, D, T, and $\ell n p_*$ having the same temporal behavior. The number of such modes is a function of the model's resolution, vertical and horizontal. In order to determine all possible modal oscillations, a linear model version must be first determined and cast in spectral form. For separability of variables, we consider perturbations about a resting atmosphere. The basic state vertical temperature profile is specified by a U.S. Standard Atmosphere.

We begin with the linearized vorticity equation:

$$\frac{\partial \zeta}{\partial t} = - \nabla \cdot f\vec{v} \,. \tag{38}$$

Letting $\xi = \nabla^2 \psi'$, $D = \nabla^2 \chi'$, $\psi' = a^2 \psi$, $\chi' = a^2 \chi$, (39)

equation (38) can be written as

$$\frac{\partial \zeta}{\partial t} = - 2\Omega \Big(D \sin\phi + \frac{\partial \psi}{\partial \lambda} + \cos\phi \, \frac{\partial \chi}{\partial \phi} \Big). \tag{40}$$

The spectral form of equation (40) is obtained by substituting the spherical harmonic expansions of the dependent variables, multiplying by the conjugate harmonic of the desired component and integrating over the sphere. After some manipulation, the spectral linear vorticity equation in each model layer reads:

$$\frac{\partial \zeta_n^\ell}{\partial t} = 2\Omega\left(\frac{i\ell}{n(n+1)}\zeta_n^\ell - \frac{n+1}{n}\varepsilon_n^\ell D_{n-1}^\ell - \frac{n}{n+1}\varepsilon_{n+1}^\ell D_{n+1}^\ell\right) . \tag{41}$$

We now turn to the linearized divergence equation

$$\frac{\partial D}{\partial t} = \vec{k} \cdot \nabla \times f \vec{v} - \nabla^2\left(\Phi + R T_o \ell n\, p_*\right) . \tag{42}$$

The geopotential Φ in equation (42) does not include its orographic component. The effects of mountains are introduced during the initialization through the nonlinear part of the divergence tendency.

In order to simplify the vertical separation of variables we define the composite variable

$$W = \Phi + RT_o \ell n\, p_* \tag{43}$$

Using the notation in equation (39), the linear divergence equation may be written

$$\frac{\partial D}{\partial t} = -2\Omega\left(-\xi \sin\phi + \frac{\partial \chi}{\partial \lambda} - \cos\phi \frac{\partial \psi}{\partial \phi}\right) - \nabla^2 W . \tag{44}$$

Inspecting equations (40) and (41) and recognizing their analogy with equation (44), the spectral form of the linearized divergence equation may be written for each model layer:

$$\frac{\partial D_n^\ell}{\partial t} = 2\Omega\left(\frac{i\ell}{n(n+1)}D_n^\ell + \frac{n+1}{n}\varepsilon_n^\ell \zeta_{n-1}^\ell + \frac{n}{n+1}\varepsilon_{n+1}^\ell \zeta_{n+1}^\ell\right) + \frac{n(n+1)}{a^2} W_n^\ell . \tag{45}$$

To close the system of equations, the linear thermodynamic and continuity equations are needed. These are

$$\frac{\partial \tilde{T}}{\partial t} = \underline{B}\, \tilde{D} , \tag{46}$$

and

$$\frac{\partial}{\partial t} \ell n\, p_* = -\sum_{k=1}^{K} \Delta_k D_k = -\Delta \tilde{D} . \tag{47}$$

Equations (46) and (47) can now be used to express the composite variable W in terms of T and D. Consider the tendency of W. Using the definition (43) we may write

$$\frac{\partial \tilde{W}}{\partial t} = \frac{\partial \tilde{\Phi}}{\partial t} + R \tilde{T}_o \frac{\partial}{\partial t} \ell n\, p_* . \tag{48}$$

Substituting from equations (46) and (47) and using the hydrostatic relation $\tilde{\Phi} = \underline{A}\,\tilde{T}$, equation (48) takes the form

$$\frac{\partial \tilde{W}}{\partial t} = (\underline{A}\,\underline{B} - R\tilde{T}_o\,\Delta)\tilde{D}. \tag{49}$$

The definition of the composite variable W thus allows us to deal with only one vertically coupled equation. Let $\underline{G} = \underline{A}\,\underline{B} - R\,\tilde{T}_o\,\Delta$,.

Since $\frac{\partial \tilde{W}}{\partial t}$ is linear in $\tilde{D}$, we may write

$$\frac{\partial \tilde{W}_n^{\ell}}{\partial t} = \underline{G}\,\tilde{D}_n^{\ell} \quad . \tag{50}$$

Equation (50) closes the system of linearized model equations.

In order to effect a separation of variables it is natural to expand all pertinent vertical column vectors in the basis vectors defined by the eigenvectors of the vertical coupling matrix G. Let $F = (F_1 \ldots F_k)$ be an arbitrary vector and $\gamma_j = (\gamma_{j1} \ldots \gamma_{jK})$, $j = 1 \ldots K$, be the eigenvectors of $\underline{G}$.

We write the eigenvector expansion

$$F = \sum_{j=1}^{K} a_j \gamma_j \ , \tag{51}$$

and need to specify the coefficients a_j. Since $\underline{G}$ is not generally symmetric, the γ_j are not orthonormal; they are, however, orthogonal to the eigenvectors γ_j', of $\tilde{\underline{G}}$, if the eigenvalues of $\underline{G}$ are distinct. Therefore

$$a_j = (F \cdot \tilde{\gamma}_j')/(\gamma \cdot \tilde{\gamma}_j') \ . \tag{52}$$

Equations (51) and (52) will be used to separate the linear solutions of equations (41), (45), and (50) as well to express tendencies in the initialization procedure. To complete the normal modes computation, let $-(gh)_j$ be the eigenvalues of $\underline{G}$. Equation (50) may then be written as

$$\frac{\partial \tilde{W}_n^{\ell}}{\partial t} = -\,(gh)_j\,\tilde{D}_n^{\ell} \quad , \quad j = 1 \ldots K \ , \tag{53}$$

and the separation of equation (50) has been accomplished.

We now note that equations (41), (45), and (53) are invariant under a substitution of all column vectors by their eigenvector expansions. The resulting equations hold for the expansion coefficients. If we assume that a given mode behaves in time according to $e^{i\omega t}$, we may continue to deal with equations (41), (45), and (53) and consider their solutions multiplied by $e^{i\omega t}$, the model's normal modes.

The matrices arising from equations (41), (45), and (53) are not symmetric and therefore do not possess orthonormal eigenvectors. The scaling

$$\xi'^{\ell}_n = \frac{\xi^{\ell}_n}{\sqrt{n(n+1)}}, \quad D'^{\ell}_n = \frac{i\, D^{\ell}_n}{\sqrt{n(n+1)}}, \quad W'^{\ell}_n = \frac{W^{\ell}_n}{a\sqrt{gh}} \tag{54}$$

leads to symmetric matrices relating the primed variables. Applying this scaling to equations (41), (45), and (53), we find

$$\frac{1}{2\pi i}\frac{\partial \zeta^{\ell}_n}{\partial t} = \frac{\ell}{n(n+1)}\zeta'^{\ell}_n + \left[\frac{n+1}{n}\left(\frac{n-1}{n+1}\right)^{\frac{1}{2}} \varepsilon^{\ell}_n D'^{\ell}_{n-1} + \frac{n}{n+1}\left(\frac{n+2}{n}\right)^{\frac{1}{2}} \varepsilon^{\ell}_{n+1}\, D'^{\ell}_{n+1}\right], \tag{55}$$

$$\frac{1}{2\pi i}\frac{\partial D'^{\ell}_n}{\partial t} = \frac{\ell}{n(n+1)}D'^{\ell}_n + \left[\frac{n+1}{n}\left(\frac{n-1}{n+1}\right)^{\frac{1}{2}} \varepsilon^{\ell}_n \xi'^{\ell}_n + \frac{n}{n+1}\left(\frac{n+2}{n}\right)^{\frac{1}{2}} \varepsilon^{\ell}_{n+1}\, \zeta'^{\ell}_{n+1}\right] + \frac{\sqrt{n(n+1)gh}}{2\Omega a} W'^{\ell}_n, \tag{56}$$

$$\frac{\partial}{\partial t} W'^{\ell}_n = \frac{i\sqrt{n(n+1)gh}}{a} D'^{\ell}_n . \tag{57}$$

Equations (55), (56) and (57) may be written in matrix form:

$$\begin{aligned}
\frac{\partial \tilde{\zeta}^{\ell}_n}{\partial t} &= i\, \underline{E}_1\, \tilde{\zeta}'^{\ell}_n + i\, \underline{E}_2 \tilde{D}'^{\ell}_n \\
\frac{\partial \tilde{D}'^{\ell}_n}{\partial t} &= i\, \underline{E}_1 \tilde{D}'^{\ell}_n + i\, \underline{E}_2 \tilde{\zeta}'^{\ell}_n + i\, \underline{E}_3 \tilde{W}'^{\ell}_n \\
\frac{\partial \tilde{W}'^{\ell}_n}{\partial t} &= i\, \underline{E}_3 \tilde{D}'^{\ell} .
\end{aligned} \tag{58}$$

Let

$$\tilde{X}^{\ell}_n = \begin{pmatrix} \tilde{\xi}'^{\ell}_n \\ \tilde{D}'^{\ell}_n \\ \tilde{W}'^{\ell}_n \end{pmatrix}, \quad \underline{E} = \begin{pmatrix} \underline{E}_1 & \underline{E}_2 & \\ \underline{E}_2 & \underline{E}_1 & \underline{E}_3 \\ & \underline{E}_3 & \end{pmatrix}, \tag{59}$$

then

$$\frac{\partial \tilde{X}^{\ell}_n}{\partial t} = i\, \underline{E}\, \tilde{X}^{\ell}_n . \tag{60}$$

The horizontal eigenvalue problem may now be written as

$$\omega \tilde{X}_n^{\ell} = \underline{E}\, \tilde{X}_n^{\ell}, \quad |\underline{E} - \omega \underline{I}| = 0 \ . \tag{61}$$

Note that matrix $\underline{E}_3$ depends on the eigenvalues of $\underline{G}$ and therefore equation (61) must be solved for each eigenvalue of matrix $\underline{G}$. The symbol $-(gh)_j$ is chosen to reflect the analogy of the shallow water problem with a nonrotating earth version of the linear model. For $\Omega = 0$, equations (44) and (50) combine to produce the wave equations with speed $\sqrt{-gh}$. It is pointed out that for positive eigenvalues of $\underline{G}$ the semi-implicit computation would be unstable.

Some of the numerical results obtained for the vertical and horizontal modes are displayed in table 1; this table displays the periods of selected horizontal gravity modes as functions of vertical modes 1 through 8 and various zonal wave numbers.

At this point, the tools required to implement a nonlinear normal modes Machenhauer initialization have been assembled. The procedure consists of the following steps: Initial data, computed in the pressure to sigma step, are transferred to the model and the full tendencies of the model's variables are calculated. These tendencies are transformed into variables analogous to those used in the normal modes computation, namely the composite variable, and scaled, primed variables. At this stage, the transformed tendencies are expanded in terms of normal modes, precomputed in permanent files, and the changes to gravity modes with periods less than 2 days are computed. These changes, $\Delta G_m = -\frac{1}{i\omega} G_m$, where G_m represents a given gravity mode with period $T = \frac{2\pi}{\omega}$ are transformed back to the model's variables and are used to adjust the input data. This process does not ensure the vanishing of gravity modes' tendencies in a subsequent tendency computation due to the nonlinear nature of the problem. It was experimentally determined that two iterations using four vertical modes produce acceptable changes in the initial conditions and very smooth surface pressure time integrations. An illustration of the initialization stabilizing effects is provided in figure 2. The surface pressure trace at a point over the Rocky Mountains is shown with and without initialization. Additional evidence of gravity waves activity in forecasts from raw and initialized data is shown in figure 3. In this figure the RMS divergence behavior demonstrates large changes with time when unbalanced initial conditions are used. Forecasts made from initialized data, portrayed by the solid graph, show much smoother behavior.

It is pointed out that the ultimate criterion for including normal modes initialization is the quality of the final forecast. The need for initialization may therefore depend on the application. For short forecasts, used in data assimilation procedures with a 6-hr cycle, the benefits of initialization may be more obvious than those obtainable in medium-range forecasting. In very short range forecasts, the adjustment period is insufficient to allow a balanced state to be reached and

oscillations in the surface pressure alone can cause rather large errors in the model's product. In medium and longer range predictions, reasonable balance can be achieved without initialization and gravitational oscillations can be damped effectively. In such forecasts the beneficial effects of initialization may be found in more appealing initial jet structures, as well as in their maintenance with time.

An evaluation of 10 forecasts produced by a rhomboidal 30,12 level spectral model using normal modes initialization was carried out by NMC's Systems Evaluation Branch. The evaluation does not attempt to investigate the influence of initialization alone, since its main purpose was to compare the operational seven-layer primitive equations model (7L PE) with the spectral system. It appears that the intensity and maintenance of the jet stream is better handled by the spectral model with normal modes initialization.

In June 1980 the Data Assimilation Final Cycle (D.A.C.) at NMC began using a spectral model to provide a "first guess" to the subsequent gridpoint analysis. The preimplementation tests included normal modes initialization and the combined product was deemed suitable for operational use in the D.A.C.

5. ACKNOWLEDGMENT

The author expresses his sincere gratitude to the staff members of the National Meteorological Center. Special thanks are expressed to N. A. Phillips for his many valuable suggestions and his assistance with the convection codes. Thanks are due to J. A. Brown, Jr. for his contribution in discussions of the vertical finite differencing problem; to J. B. Hovermale for his efforts in evaluating various parameterization techniques; to J. D. Stackpole for conducting a comprehensive objective evaluation of the model, to J. P. Gerrity and R. D. McPherson for assistance in data problems; to R. E. Livezey for assisting in the convective adjustment algorithm; to D. F. Parrish for his FFT optimization efforts; to J. F. O'Connor for his detailed comparison and evaluation of the model; to M. J. Rozwodoski for sharing his comprehensive computer expertise; to B. Ballish for his work with the normal modes initialization; and to Joyce Peters for typing this manuscript.

6. REFERENCES

Arakawa, A., and Y. Mintz, 1974: The UCLA Atmospheric Circulation Model, Department of Meteorology, University of California.

Ballish, A. B., 1980: Initialization, theory and application to the NMC spectral model. Doctoral Dissertation, University of Maryland.

Bourke, W., 1974: A multi-level spectral model. Formulation and hemispheric integrations. Mon. Wea. Rev., 102, 687-701.

Brown, J. A., 1974: On vertical differencing in the sigma system. NMC Office Note 92, U.S. Department of Commerce, NOAA, NWS, Washington, DC.

Cressman, G., 1960: Improved terrain effects in barotropic forecasts. Mon. Wea. Rev., 88, 327-342.

Eliasen, E., B. Machenhauer, and E. Rasmusen, 1970: On a numerical method for integration of the hydrodynamic equations with a spectral representation of the horizontal fields. Institute for Theoretical Meteorology, University of Copenhagen, Report No. 2, Copenhagen, Denmark.

Flattery, T. W., 1967: Hough functions. The University of Chicago, Dept. of Geophysical Sciences. Technical Report No. 20 to the National Science Foundation, March 1976.

Gerrity, J. P., 1976: The LFM Model - 1976: A documentation. NOAA Technical Memorandum NWS NMC 60, U.S. Department of Commerce, Washington, DC.

Hughes, F., 1981: Skill of the Medium Range Forecast Group, NMC Office Note 227, U.S. Department of Commerce, NOAA, NWS, Washington, DC.

Kistler, R., and D. Parrish: An improved data assimilation system at NMC. Manuscript in preparation.

Krylov, V. I., 1962: Approximate calculation of integrals, ACM Monograph Series, The MacMillan Company, New York, NY.

Kuo, H.L., 1965: On formation and intensification of tropical cyclones through latent heat release by cumulus convection. J. Atmos. Sci., 22, 40-63.

Machenhauer, B. and E. Rasmussen, 1972: On the integration of the spectral hydrodynamical equations by a transform method. Institute for Theoretical Meteorology, University of Copenhagen, Report No. 3, Copenhagen, Denmark.

Machenhauer, B., 1977: On the dynamics of gravity oscillations in a shallow water model, with applications to normal mode initialization. Beitrage zur Physik der Atmosphäre, 50, pp. 253-271.

Orszag, S. A., 1970: Transform methods for calculation of vector coupled sums: Application to the spectral form of the vorticity equations. J. Atmos. Sci., 27, 890-895.

Phillips, N. A., 1959: Numerical integration of the primitive equation on the hemisphere. Mon. Wea. Rev., 87, 333-345.

_____, 1974: Application of Arakawa's energy conserving layer model to operational numerical weather prediction. NMC Office Note 104, August 1975, U.S. Department of Commerce, NOAA, NWS.

_____, 1979: The Nested Grid Model. NOAA Tech. Report NWS-22, U.S. Department of Commerce, NOAA, NWS.

Robert, A. J., 1965: The behavior of planetary waves in an atmosphere model based on spherical harmonics. Arctic Meteor. Res. Group, McGill University Publ. Meteor., No. 77, pp. 59-62.

_____ , 1969: Integration of a spectral model of the atmosphere by the implicit method. Proc. WMO/IUGG Symposium on Numerical Weather Prediction, Tokyo, 26 November - 4 December 1968. Japan Meteorological Agency, Tokyo.

Roll Hill, 1965: Physics of the marine atmosphere. Academic Press, 426 pp.

Shuman, F., and J. Hovermale, 1968: An operational six-layer primitive equation model, J. App. Met., 7, 525-547.

Stackpole, J., 1980: How to pick another new forecast model, (Spectral vs. 7L PE), NMC Office Note 215, U.S. Department of Commerce, NOAA, NWS.

_____, 1978: The NMC 9-Layer Global Primitive Equation Model on a latitude-longitude grid. NMC Office Note 178, U.S. Department of Commerce, NOAA. NWS.

7. APPENDIX A - THE ARAKAWA VERTICAL FINITE DIFFERENCING SCHEME

The Arakawa vertical finite differencing scheme is derived by writing the energy equation in the continuous and discretized forms. The requirement that both forms be similar leads to the finite differencing form of the hydrostatic equation.

We begin with the continuous equations. The momentum equations in flux form in the sigma coordinate system are

$$\frac{\partial p_* u}{\partial t} + \nabla\cdot p_* u\vec{v} + \frac{\partial}{\partial\sigma}(p_* u\dot{\sigma}) = -\frac{\partial}{\partial x}(p_*\Phi) - \frac{\partial}{\partial\sigma}[(1-\sigma)\Phi]\frac{\partial p_*}{\partial x} + p_* fv, \quad (A.1)$$

$$\frac{\partial p_* v}{\partial t} + \nabla\cdot p_* v\vec{v} + \frac{\partial}{\partial\sigma}(p_* v\dot{\sigma}) = -\frac{\partial}{\partial y}(p_*\Phi) - \frac{\partial}{\partial\sigma}[(1-\sigma)\Phi]\frac{\partial p_*}{\partial y} - p_* fu. \quad (A.2)$$

The vertical finite differencing considerations are independent of the choice of horizontal coordinates. Using the continuity equation

$$p_* \frac{\partial\dot{\sigma}}{\partial\sigma} + \frac{\partial p_*}{\partial t} + \nabla\cdot p_*\vec{v} = 0, \quad (A.3)$$

the kinetic energy equation is derived:

$$\frac{\partial p_* k_e}{\partial t} + \nabla\cdot p_*(\Phi+k_e)\vec{v} + \frac{\partial}{\partial\sigma} p_*\dot{\sigma}(\Phi+k_e) - \frac{\partial}{\partial\sigma}\left(\Phi\frac{\partial p}{\partial t}\right) = -\dot{p}\frac{\partial\Phi}{\partial\sigma}. \quad (A.4)$$

In equation (A.4), $k_e = \frac{1}{2}(\vec{v}\cdot\vec{v})$ is the kinetic energy per unit mass, p is the pressure divided by 100 cb, and $\dot{p}$ its substantial derivative.

To complete the energy equation, we add the thermodynamic equation,

$$\frac{\partial p_* C_p T}{\partial t} + \nabla\cdot p_* C_p T\vec{v} + \frac{\partial}{\partial\sigma} p_* C_p T\dot{\sigma} = p_* C_p\theta\frac{d\pi}{dt} \quad (A.5)$$

to the kinetic energy equation (A.4) to obtain

$$\frac{\partial p_*(k_e+C_pT)}{\partial t} - \frac{\partial}{\partial\sigma}\left(\Phi\frac{\partial p}{\partial t}\right) + \nabla\cdot p_*(k_e+C_pT+\Phi)\vec{v} + \frac{\partial}{\partial\sigma} p_*\dot{\sigma}(k_e+C_pT+\Phi) = p_*\left[C_p\theta\frac{d\pi}{dt} - \frac{\partial\Phi}{\partial\sigma}\frac{dp}{dt}\right] = 0. \quad (A.6)$$

In the last equations, $\theta = \frac{T}{\pi}$, $\pi = p^{\kappa}$, $\kappa = \frac{R}{c_p}$. The vanishing of the right-hand side in equation (A.6) is a consequence of the hydrostatic assumption.

We now turn to the discretized equations using, at this point, values at interfaces as well as layers. For layer k, we express (A.1) and (A.2) as

$$\frac{\partial p_* u_k}{\partial t} + \nabla \cdot p_* u_k \vec{v}_k + \frac{p_*}{\Delta_k}\left(\hat{u}_{k+1}\,\dot{\hat{\sigma}}_{k+1} - \hat{u}_k\,\dot{\hat{\sigma}}_k\right) = -\frac{\partial}{\partial x}(p_*\Phi_k),$$
$$-\frac{1}{\Delta_k}\left(\hat{S}_{k+1}\,\hat{\Phi}_{k+1} - \hat{S}_k\hat{\Phi}_k\right)\frac{\partial p_*}{\partial x} + p_* f v_k \tag{A.7}$$

$$\frac{\partial p_* v_k}{\partial t} + \nabla \cdot p_* v_k \vec{v}_k + \frac{p_*}{\Delta_k}\left(\hat{v}_{k+1}\,\dot{\hat{\sigma}}_{k+1} - \hat{v}_k\,\dot{\hat{\sigma}}_k\right) = -\frac{\partial}{\partial y}(p_*\Phi_k),$$
$$-\frac{1}{\Delta_k}\left(\hat{S}_{k+1}\,\hat{\Phi}_{k+1} - \hat{S}_k\,\hat{\Phi}_k\right)\frac{\partial p_*}{\partial y} - p_* f u_k \tag{A.8}$$

where

$$\hat{S}_k = 1 - \hat{\sigma}_k. \tag{A.9}$$

Defining

$$\pi_k = \frac{T_k}{\theta_k} \tag{A.10}$$

and multiplying the thermodynamic equation $c_p\pi_k$, we have

$$\frac{\partial}{\partial t} p_* C_p T + \nabla \cdot p_* C_p T_k \vec{v}_k + \frac{p_* C_p}{\Delta_k}\left(\dot{\hat{\sigma}}_{k+1}\,\hat{T}_{k+1} - \dot{\hat{\sigma}}_k \hat{T}_k\right) =$$
$$p_* C_p \theta_k\left(\frac{\partial \pi_k}{\partial t} + \vec{v}_k \cdot \nabla \pi_k\right) + \frac{p_* C_p}{\Delta_k}\left[\dot{\hat{\sigma}}_{k+1}\left(\hat{T}_{k+1} - \pi_k \hat{\theta}_{k+1}\right) - \dot{\hat{\sigma}}_k\left(\hat{T}_k - \pi_k \hat{\theta}_k\right)\right]. \tag{A.11}$$

The total energy equation is now obtained by combining equations (A.7), (A.8), and (A.11) in a manner similar to the continuous case; it reads

$$\frac{\partial}{\partial t}(k_{ek} + C_p T_k) p_* - \frac{1}{\Delta_k}\left(\hat{\Phi}_{k+1}\frac{\partial}{\partial t}\hat{p}_{k+1} - \Phi_k \frac{\partial \hat{p}_k}{\partial t}\right) + \nabla \cdot p_* \vec{v}_k \left(k_{ek} + C_p T_k + \Phi_k\right)$$
$$+ \frac{p_*}{\Delta_k}\left[\dot{\hat{\sigma}}_{k+1}\left(\tfrac{1}{2}\vec{v}_k \cdot \vec{v}_{k+1} + C_p \hat{T}_{k+1} + \hat{\Phi}_{k+1}\right) - \dot{\hat{\sigma}}_k\left(\tfrac{1}{2}\vec{v}_k \cdot \vec{v}_{k-1} + C_p \hat{T}_k + \hat{\Phi}_k\right)\right] =$$
$$\frac{p_*}{\Delta_k}\left(\dot{\hat{\sigma}}_{k+1}\left[\hat{\Phi}_{k+1} - \Phi_k + C_p\left(\hat{T}_{k+1} - \pi_k \hat{\theta}_{k+1}\right)\right] - \dot{\hat{\sigma}}_k\left[\hat{\Phi}_k - \Phi_k + C_p\left(\hat{T}_k - \pi_k \hat{\theta}_k\right)\right]\right) \tag{A.12}$$
$$+ C_p p_* \theta_k\left(\frac{\partial \pi_k}{\partial t} + \vec{v}_k \cdot \nabla \pi_k\right) + \frac{1}{\Delta_k}\left(\frac{\partial p_*}{\partial t} + \vec{v}_k \cdot \nabla p_*\right)\left[\Phi_k\left(\hat{S}_{k+1} - \hat{S}_k\right)\right.$$
$$\left. - \left(\hat{\Phi}_{k+1}\,\hat{S}_{k+1} - \hat{\Phi}_k \hat{S}_k\right)\right].$$

Equation (A.12) would be analogous to the continuous energy equation (A.6) if the right-hand side vanished for all layers, and for all possible $\dot{\sigma}_k$. This would occur if

$$\hat{\Phi}_{k+1} - \Phi_k + C_p\left(\hat{T}_{k+1} - \pi_k\,\hat{\theta}_{k+1}\right) = 0 \qquad k=1,\ldots,K-1 \qquad (A.13)$$

$$\hat{\Phi}_k - \Phi_k + C_p\left(\hat{T}_k - \pi_k\hat{\theta}_k\right) = 0 \qquad k=2,\ldots,K \qquad (A.14)$$

and for $k = 1,\ldots,K$

$$C_p p_* \theta_k\left(\frac{\partial \pi_k}{\partial t} + \vec{v}_k\cdot\nabla\pi_k\right) + \frac{1}{\Delta_k}\left(\frac{\partial p_*}{\partial t} + \vec{v}_k\cdot\nabla p_*\right)\left[\Phi_k\left(\hat{S}_{k+1} - \hat{S}_k\right) - \left(\hat{\Phi}_{k+1}\hat{S}_{k+1} - \hat{\Phi}_k\hat{S}_k\right)\right] = 0. \qquad (A.15)$$

It can be shown that following Arakawa and writing $\theta_k = \frac{1}{2}(\theta_k + \theta_{k-1})$, θ^2 will be conserved in time, with similar results for other variables so related. With this specification for the interface potential temperatures, equations (A.13) and (A.14) for $k = 2,\ldots,K$ reduce to

$$\begin{aligned}\hat{\Phi}_k - \Phi_{k-1} + C_p\left[\hat{T}_k - \frac{\pi_{k-1}}{2}\left(\frac{T_k}{\pi_k} + \frac{T_{k-1}}{\pi_{k-1}}\right)\right] &= 0,\\ \hat{\Phi}_k - \Phi_k + C_p\left[\hat{T}_k - \frac{\pi_k}{2}\left(\frac{T_k}{\pi_k} + \frac{T_{k-1}}{\pi_{k-1}}\right)\right] &= 0.\end{aligned} \qquad (A.16)$$

$\hat{\Phi}_k$ and $\hat{T}_k$ are easily eliminated from equations (A.16) leaving a relation between layer temperatures and layer geopotentials. To close the system, equation (A.15) is manipulated using the Brown (1974) and Phillips (1974) specification of layer pressures

$$\pi_k = \frac{\hat{p}_k^{1+\kappa} - \hat{p}_{k+1}^{1+\kappa}}{(1+\kappa)\left(\hat{p}_k - \hat{p}_{k+1}\right)} \sim \frac{1}{(1+\kappa)}\,\frac{d}{dp}\,p^{(1+\kappa)} \qquad (A.17)$$

to obtain, for $k = 1,\ldots,K$

$$RT_k + \frac{1}{\Delta_k}\left[\Phi_k\left(\hat{S}_{k+1} - \hat{S}_k\right) - \left(\hat{\Phi}_{k+1}\hat{S}_{k+1} - \hat{\Phi}_k\hat{S}_k\right)\right] = 0. \qquad (A.18)$$

When equation (A.18) is summed over all layers and $\hat{\Phi}_1$ identified as the fixed geopotential at the ground, we have

$$R\sum_{k=1}^{K}\Delta_k\,T_k = \sum_{k=1}^{K}\Delta_k\,\phi_k - \hat{\phi}_1\,, \qquad (A.19)$$

thus completing the finite difference version of the hydrostatic equation.

The transformation of the equations from flux form to the form used in the model's formulation is straightforward.

8. APPENDIX B - BASIC SPECTRAL CONCEPTS

We are considering scalar functions of position on a sphere, expressed as truncated spherical harmonic expansions. Let $x=\sin\phi$. Then for the purposes of this report, the Legendre polynomials are defined as

$$P_n^\ell(x) = \frac{(-1)^{\ell+n}}{2^n\, n!} \left[\frac{(2n+1)\,(n-\ell)!}{2(n+\ell)!}\right]^{\frac{1}{2}} (1-x^2)^{\ell/2}\, \frac{d^{\ell+n}}{dx^{\ell+n}}\, (1-x^2)^n. \qquad \text{(B.1)}$$

The normalization implied by equation (B.1) is such that

$$\int_{-1}^{1} P_n^\ell(x)\, P_m^\ell\, dx = \delta_{m,m}. \qquad \text{(B.2)}$$

Here ℓ and n are the zonal and ordinal wave numbers respectively. The generation of numerical values for P_n^ℓ is based on the recursion relation

$$xP_n^\ell(x) = \varepsilon_{n+1}^\ell\, P_{n+1}^\ell(x) + \varepsilon_n^\ell\, P_{n-1}^\ell(x), \qquad \text{(B.3)}$$

where

$$\varepsilon_n^\ell = \left[\frac{n^2-\ell^2}{4n^2-1}\right]^{\frac{1}{2}}. \qquad \text{(B.4)}$$

The numerical computation is performed in double precision. For purposes of differentiation, we use

$$(1-x^2)\, \frac{d\, P_n^\ell}{dx} = (n+1)\, \varepsilon_n^\ell\, P_{n-1}^\ell - n\varepsilon_{n+1}^\ell\, P_{n+1}^\ell = \cos\phi\, \frac{d\, P_n^\ell}{d\phi}. \qquad \text{(B.5)}$$

Relation (B.5) is employed in computations deriving wind components from vorticity and divergence as well as in implementing the divergence, gradient, and curl operators in the code.

Defining a surface spherical harmonic as

$$Y_n^\ell(\phi,\lambda) = P_n^\ell(\sin\phi)\, e^{i\ell\lambda},$$

it follows that

$$\int_S Y_n^\ell \, (Y_n^\ell)^* \, ds = 2\Pi \,, \tag{B.6}$$

where S is the surface of the unit sphere and the asterisk denotes complex conjugation.

A rhomboidal spherical harmonic expansion depicted in figure 5 is defined by

$$H(\phi,\lambda) = \sum_{\ell=-J}^{J} \sum_{h=|\ell|}^{|\ell|+J} H_n^\ell \, Y_n^\ell \,. \tag{B.7}$$

If H represents any physical variable, and is therefore real, it can be shown that

$$H_n^{-\ell} = (-1)^\ell \, (H_n^\ell)^* \tag{B.8}$$

and it is sufficient to consider only coefficients with $\ell \geq 0$.

In the Large Scale Cycle, the model derives its input data from the Hough analysis (Flattery, 1967). In this analysis, Hough functions are expressed as expansions in Legendre polynomials and trigonometric functions. In order to guarantee a correct transformation of the meteorological variables from Hough to spherical harmonic expansions, we require that the two expansions produce identical series.

In the Hough analysis, height and pseudo winds $\vec{v}/\cos\phi$ are expressed as

$$H = \sum_{n=o}^{55} C_n^o P_n^o + \sum_{\ell=1}^{24} \sum_{n=\ell}^{55} (C_n^\ell \cos\ell\lambda \pm S_n^\ell \sin\ell\lambda) P_n^\ell. \tag{B.9}$$

Equation (B.9) is written with fixed upper summation limits, the plus symbol is used for the height and u component of the wind while the minus sign is used for v. Using equations (B.7) and (B.8) and equating coefficients with those in (B.9), the transformation for n=1...55. is

$$H_n^o = C_n^o$$

$$H_n^\ell = \frac{1}{2} (C_n^\ell \mp S_n^\ell) \quad \ell = 1 \ldots 24. \tag{B.10}$$

Equations (B.10) together with

$$H = \sum_{n=o}^{55} H_n^o P_n^o + 2\,\mathrm{Real}\left(\sum_{\ell=1}^{24} \sum_{n=\ell}^{55} H_n^\ell P_n^\ell \, e^{i\ell\lambda} \right) \tag{B.11}$$

ensure a correct reproduction of the Hough data in the spectral model.

At this point, it should be mentioned that the Hough analysis is very closely approximated by a J=24 rhomboidal expansion. In the higher resolution J=30 model, the unavailable higher modes are set initially to zero.

The two major ingredients of the transform method are the transition from a series representation to a gridded field and its inverse. The transform method, designed to compute the expansion of quadratic terms appearing in the forecast equations, is predicated on the ability to perform these computations efficiently, thus circumventing the interaction coefficients method used during the early stages of spectral techniques. The ability to incorporate physical effects on the transform grid, effects that do not otherwise lend themselves to a simple spectral treatment, is a fortunate consequence.

In the following, the important details of the grid to spectral and its inverse computation are examined. We begin with the grid to spectral conversion.

Let the function $H(\phi,\lambda)$ defined by equation (B.7) be given, and let it be required to compute its expansion coefficients H_n^ℓ. Multiplying (B.7) by $(Y_n^\ell)^*$, integrating over the unit sphere, and using the orthogonality condition (B.6), we have

$$H_n^\ell = \frac{1}{2\Pi} \int_S H(\phi,\lambda)(Y_n^\ell)^* ds = \frac{1}{2\Pi} \int_o^{2\Pi} \int_{-\frac{\Pi}{2}}^{\frac{\Pi}{2}} H(\phi,\lambda) P_n^\ell(\sin\phi) e^{-i\ell\lambda} \cos\phi \, d\phi \, d\lambda. \tag{B.12}$$

The numerical evaluation of the integrals in (B.12) proceeds in two steps. First, we define Fourier coefficients at the given latitude:

$$H^\ell(\phi) = \frac{1}{2\Pi} \int_o^{2\Pi} H(\phi,\lambda) e^{-i\ell\lambda} d\lambda \tag{B.13}$$

and compute them using a Fast Fourier Transform. Next, let $G_i = \dfrac{2}{(1-X_k^2)\,P^1\,(X_k)^2}$ be the Gaussian weights (Krylov, p. 108).

Then, if $y=y(x)$ is a polynomial of degree not exceeding 2N-1

$$\int_{-\frac{\Pi}{2}}^{\frac{\Pi}{2}} y(\phi)\cos\phi \, d\phi = \int_{-1}^{1} y(x)\,dx = \sum_{i=1}^{N} G_i y(x_i). \tag{B.15}$$

Using this method of integration, (B.12) may be accurately evaluated numerically by

$$\int_{-1}^{1} H^{\ell}(x)P_n^{\ell}(x)dx = \sum_{i=1}^{N} H^{\ell}(x_i)P_n^{\ell}(x_i)G_i. \qquad (B.16)$$

Figure 4 depicts the Gaussian grid defined for these integrations. The zeros of P_N determine the North-South definition of the grid, while an equally spaced resolution is used for each latitude circle. The degree of P_N is determined by the power series the integrand is assumed to possess. In the model, the accurate integration of quadratic terms arising from a rhomboidal truncation requires that $N \geq \frac{5J+1}{2}$, Machenhauer (1972), Orszag (1970). For J=30, N=76, while for J=24, N=62 Gaussian latitudes. Table 2 displays the Gaussian colatitudes and weights in the Northern Hemisphere for the J=30 case. It is noted that the poles do not appear on the grid.

The computation of grid values from the spectral definition (B.7) is straightforward and is accomplished as follows. We first write equation (B.7) as:

$$H(\phi,\lambda) = \sum_{n=o}^{J} H_n^o P_n^o + 2\,\mathrm{Re}\left(\sum_{\ell=1}^{J}\sum_{n=\ell}^{\ell+J} H_n^{\ell}P_n^{\ell}(\sin\phi)\right)e^{i\ell\lambda}. \qquad (B.17)$$

Next, the P_n are computed for the required latitude, and the sums

$$H^{\ell} = \sum_{n=\ell}^{\ell+J} H_n^{\ell}P_n^{\ell}(\sin\phi) \qquad \ell = o \ldots J \qquad (B.18)$$

are evaluated. Equation (B.17) can now be written as

$$H(\phi,\lambda) = \sum_{\ell=o}^{J} H^{\ell}e^{i\ell\lambda}, \qquad (B.19)$$

and its form suggests the application of a Fast Fourier Transform (FFT).

At this point, the FFT was mentioned in the computation of spectral coefficients from gridded data, equation (B.13), as well as in the reverse calculation, equation (B.19). In order to implement the FFT, we define

$$\hat{X}(j) = \sum_{k=o}^{M-1} X(k)\, e^{\frac{2\Pi ijk}{M}} \qquad (B.20)$$

$$X(x) = \frac{1}{M}\sum_{j=o}^{M-1} \hat{X}(j)\, e^{\frac{-2\Pi ijk}{M}}.$$

The $\hat{X}(j)$ and $X(x)$ are said to be a discrete Fourier Transform pair.

A computer algorithm to implement equations (B.20) efficiently is referred to as an FFT. A variety of such codes is now available and their optimization is computer dependent. A documentation of the FFTs used in the spectral system can be found in NMC Office Note 231.

We now return to equation (B.19) and note that λ is as yet unrelated to a grid. Inspecting equation (B.13) reveals that in order to perform a numerical integration a specification of a grid is necessary.

It can be shown that if $f(x)$ is a trigonometric polynomial of degree not exceeding M-1

$$\int_o^{2\Pi} f(x)dx = \frac{2\Pi}{M} \sum_{j=o}^{M-1} f\left(\frac{2\Pi j}{M}\right) \qquad \text{(B.21)}$$

is an exact quadrature.

In the case of equation (B.13) we anticipate trigonometric polynomials of degree up to 3J, arising in quadratic terms. For exact integrations we therefore specify $M \geq 3J+1$.

Following eq. (B.21), eq. (B.13) may now be written

$$H^{\ell}(\phi) = \frac{1}{M} \sum_{j=o}^{M-1} H(\phi,\lambda_j)\, e^{\frac{-2\Pi i \ell j}{M}} \qquad j = o \ldots (3J+1) \qquad \text{(B.22)}$$

and $\Delta\lambda = \frac{2\Pi}{3J+1}$.

Equation (B.22) is suitable for the application of an FFT. Since the implementation of any FFT is most efficient when M is rich in factors, the Gaussian Grid for J=30 was specified with 96 (>3x30+1) points while for J=24 it is efficient to specify 80 (>3x24+1) points.

The application of an FFT to equation (B.19) can now be performed by writing

$$H(\phi,\lambda_j) = \sum_{\ell=o}^{M-1} H^{\ell}\, e^{\frac{2\Pi i \ell j}{M}} . \qquad \text{(B.23)}$$

It is pointed out that $H^{\ell}=o$ for $\ell>J$ and a single application of an FFT to equation (B.23) produces values of H at all λ, for the chosen latitude ϕ.

Table 1.--GRAVITY WAVE STATISTICS.

Vertical Mode Number	Planetary Wave Number	Periods of Fastest Gravity Mode	Periods of Slowest Gravity Mode	Periods of Fastest Rossby Mode	Number of Gravity Modes With Periods in the Time Range: 0-12 hrs	12-24 hrs	24-48 hrs	48+ hrs
1	0	1.48	19.3		46	2	0	0
1	1	1.42	33.1	28.6	47	2	1	0
1	5	1.23	6.85	73.1	50	0	0	0
1	15	.917	2.35	192	50	0	0	0
1	24	.747	1.48	300	50	0	0	0
2	0	2.98	28.9		42	4	2	0
2	1	2.86	70.4	36.3	43	6	0	1
2	5	2.48	14.2	76.0	49	1	0	0
2	15	1.86	4.79	193	50	0	0	0
2	24	1.51	3.01	300	50	0	0	0
4	0	10.0	64.4		12	28	6	2
4	1	9.82	346	70.8	15	27	6	2
4	5	9.18	40.7	101	18	26	5	1
4	15	7.80	23.1	203	31	19	0	0
4	24	6.72	14.4	306	43	7	0	0
6	0	11.8	102		4	28	12	4
6	1	11.7	871	178	4	30	12	4
6	5	11.8	174	136	4	30	12	4
6	15	11.9	58.1	227	2	33	14	1
6	24	11.7	36.3	322	4	36	10	0
8	0	12.1	142		0	32	8	8
8	1	12.0	138	150	0	34	8	8
8	5	12.2	119	179	0	30	12	8
8	15	13.1	120	262	0	26	16	8
8	24	13.7	74.8	350	0	26	19	5

The above statistics are for a 12 layer, equal σ-spaced model, with truncation of 24.

Table 2.--GAUSSIAN LATITUDES AND WEIGHTS FOR J=30.

	Colatitude	Weight
1	1.80	0.1267791E-02
2	4.13	0.2949103E-02
3	6.48	0.4627932E-02
4	8.83	0.6299179E-02
5	11.18	0.7959846E-02
6	13.53	0.9607103E-02
7	15.89	0.1123817E-01
8	18.24	0.1285028E-01
9	20.59	0.1444073E-01
10	22.94	0.1600683E-01
11	25.30	0.1754593E-01
12	27.65	0.1905546E-01
13	30.00	0.2053285E-01
14	32.35	0.2197561E-01
15	34.71	0.2388132E-01
16	37.06	0.2474761E-01
17	39.41	0.2607216E-01
18	41.77	0.2735275E-01
19	44.12	0.2858722E-01
20	46.47	0.2977348E-01
21	48.82	0.3090955E-01
22	51.18	0.3199348E-01
23	53.53	0.3302347E-01
24	55.88	0.3399778E-01
25	58.24	0.3491475E-01
26	60.59	0.3577286E-01
27	62.94	0.3657064E-01
28	65.29	0.3730676E-01
29	67.65	0.3797996E-01
30	70.00	0.3858913E-01
31	72.35	0.3913322E-01
32	74.71	0.3961133E-01
33	77.06	0.4002265E-01
34	79.41	0.4036647E-01
35	81.76	0.4064223E-01
36	84.12	0.4084946E-01
37	86.47	0.4098780E-01
38	88.82	0.4105704E-01

MODEL STRUCTURE

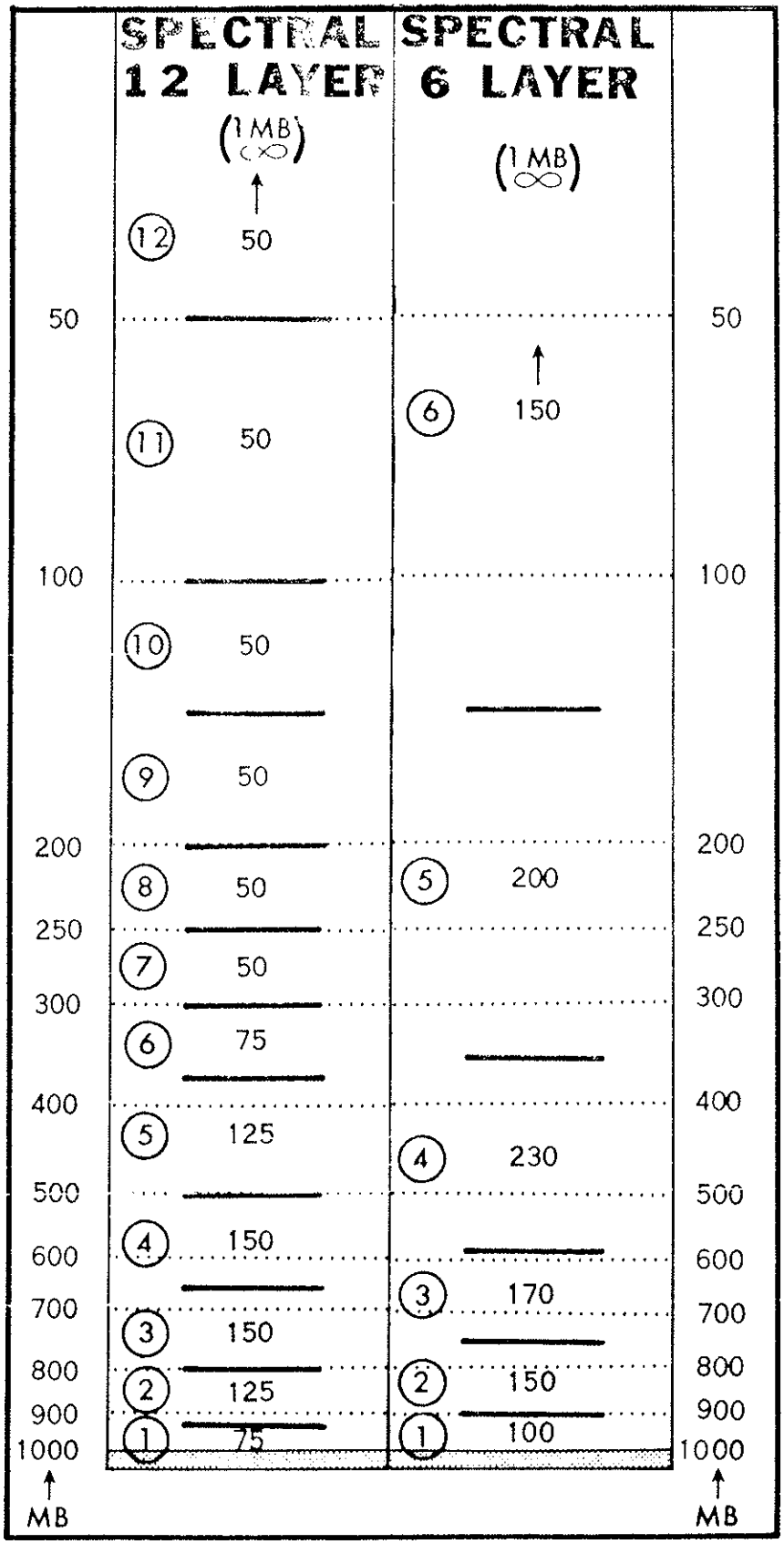

Figure 1

SURFACE PRESSURE TRACE
WITH AND WITHOUT INITIALIZATION

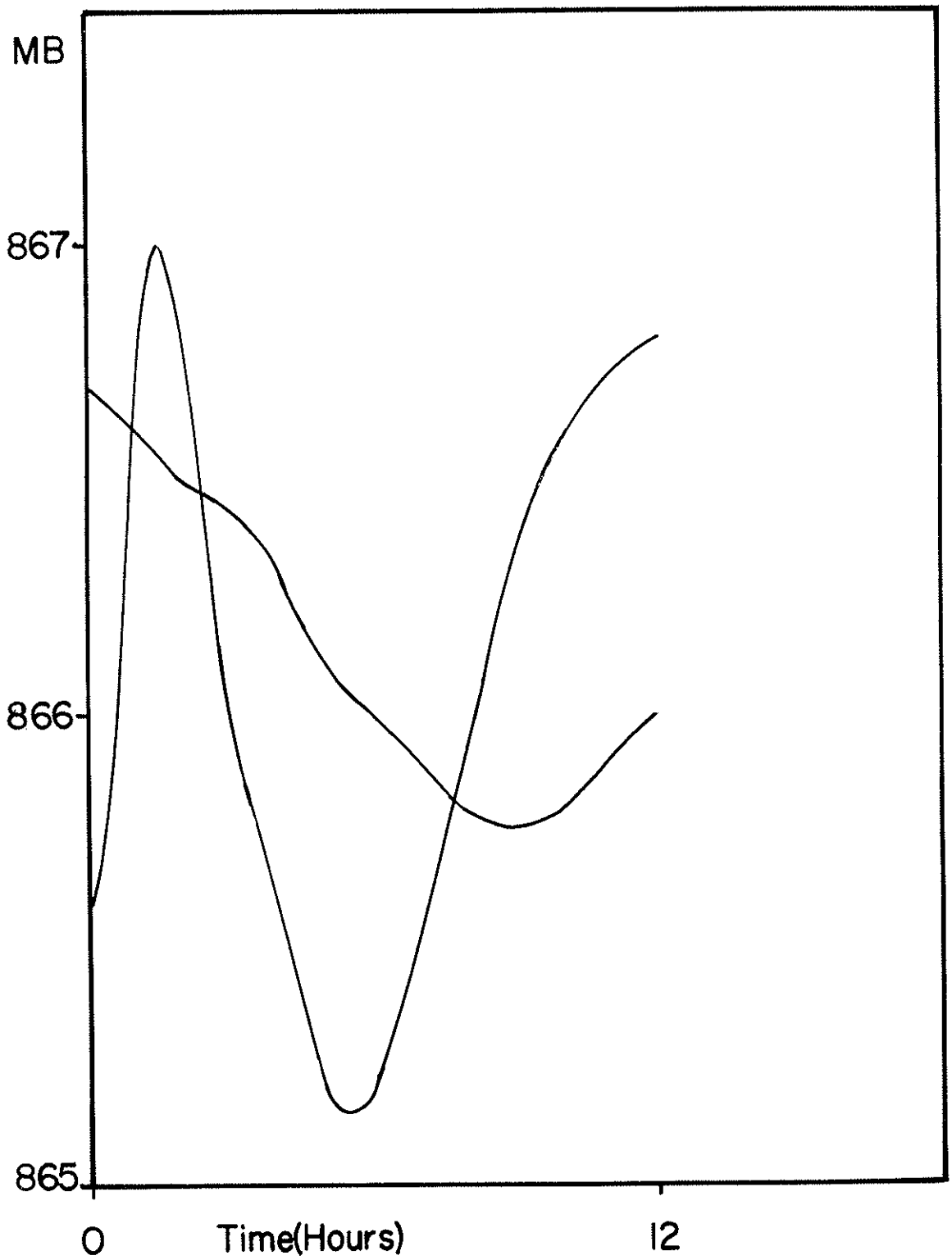

Figure 2

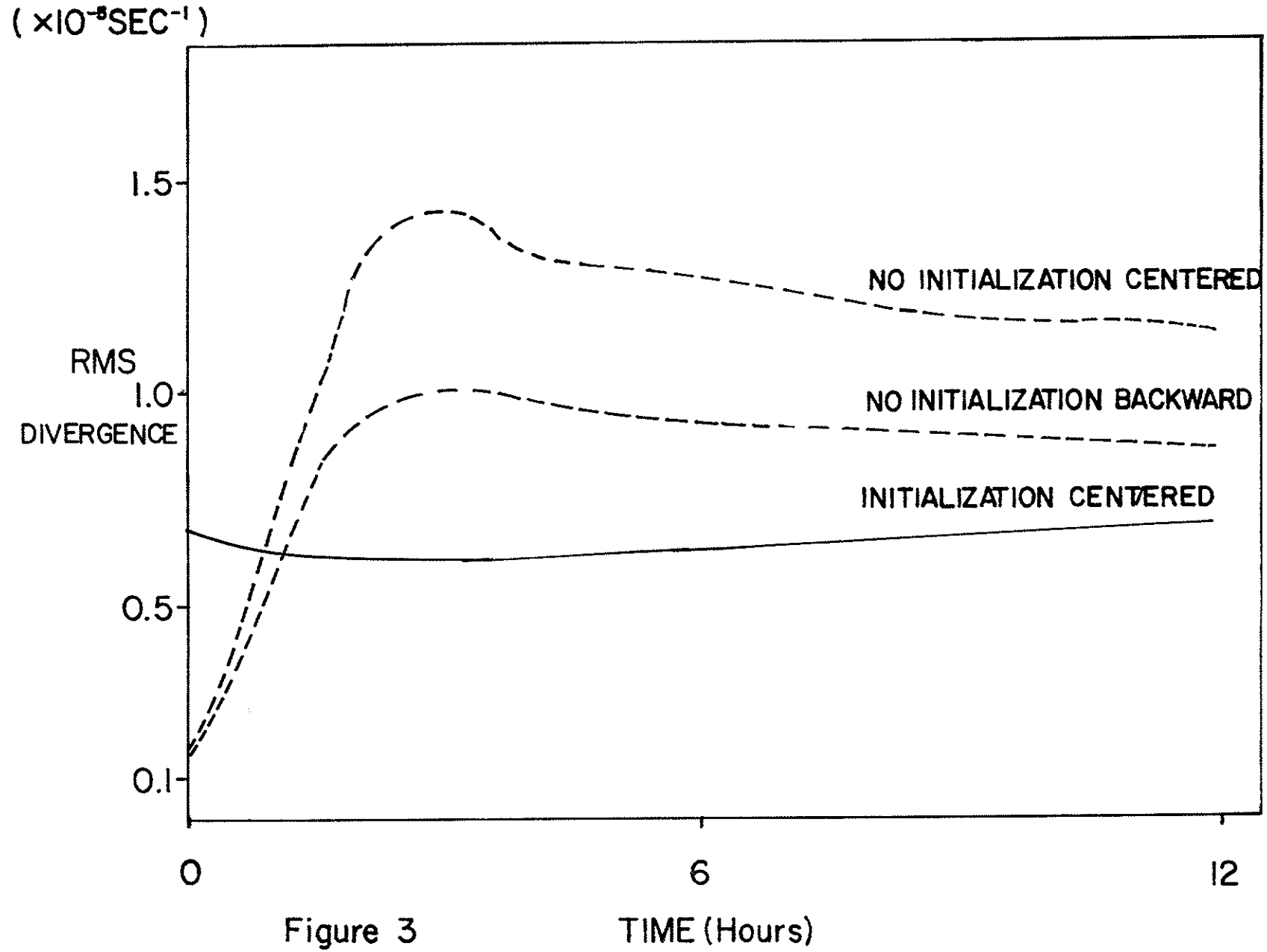
RMS DIVERGENCE TRACE
WITH AND WITHOUT INITIALIZATION
(×10⁻⁵SEC⁻¹)
1.5
RMS
1.0
DIVERGENCE
0.5
0.1
NO INITIALIZATION CENTERED
NO INITIALIZATION BACKWARD
INITIALIZATION CENTERED
0
6
12
TIME (Hours)

Figure 3

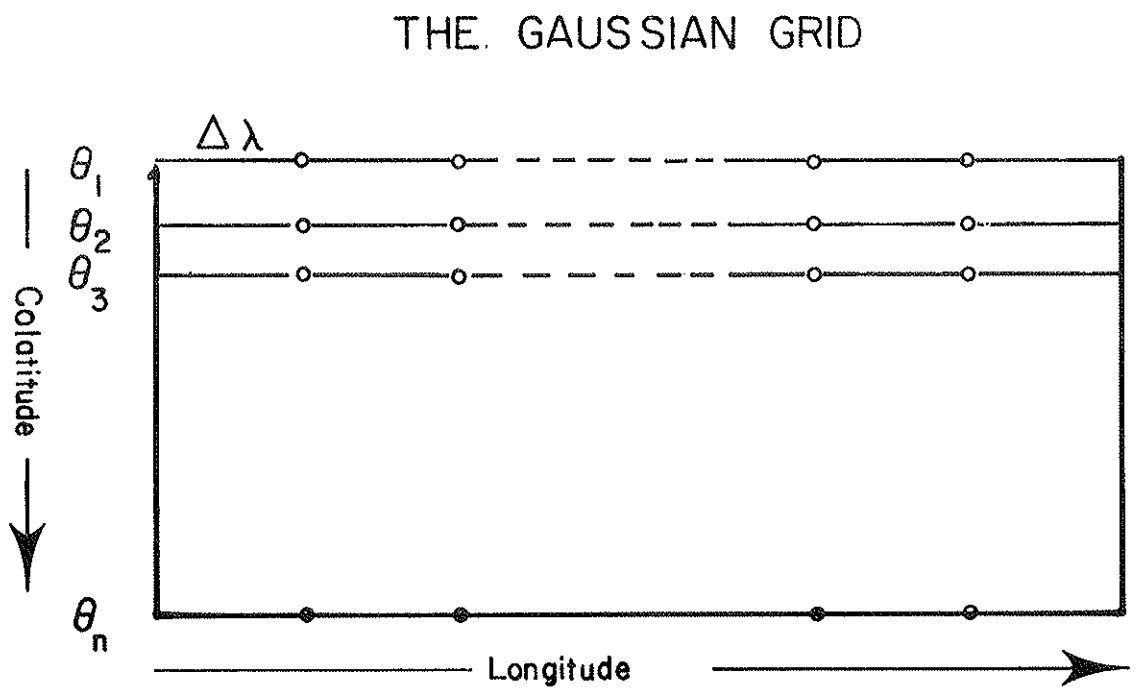

Figure 4

THE RHOMBOIDAL TRUNCATION

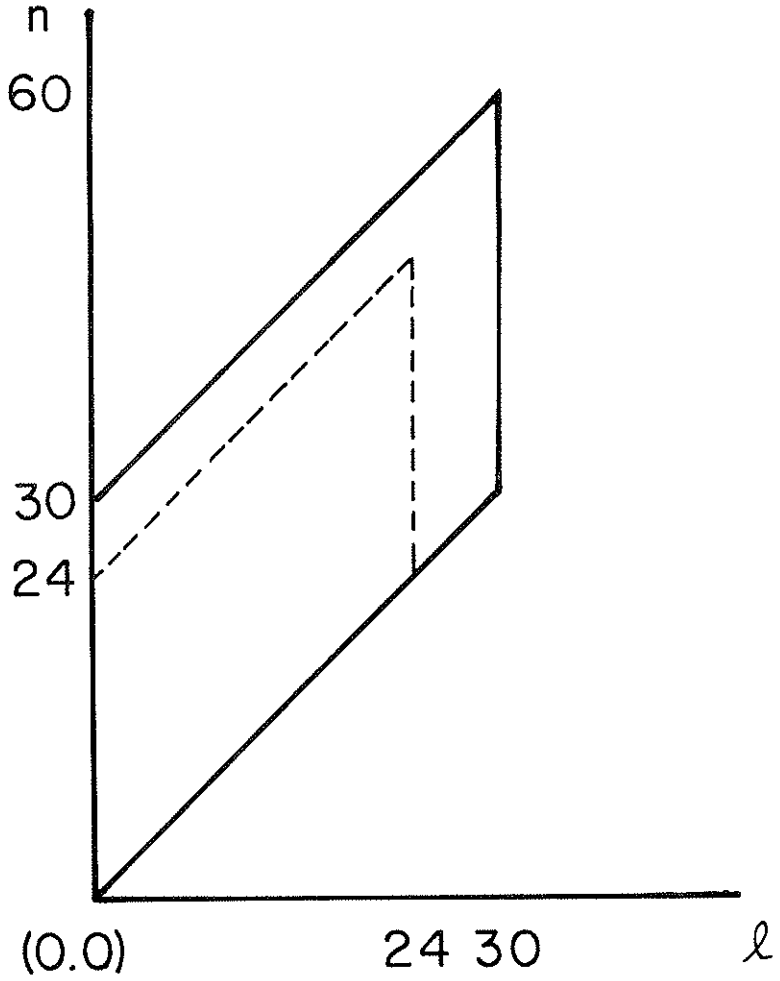

Figure 5

S1 SCORES STATISTICS

S1 comparisons of the Spectral and LFM for the continguous United States. Grid used: 49-point lat/long grid. This is a subset of a 63-point grid which covers the area between 65 west and 145 west longitude, and between 25 north and 55 north latitude. Gridpoint spacing is 5 degrees latitude by 10 degrees longitude.

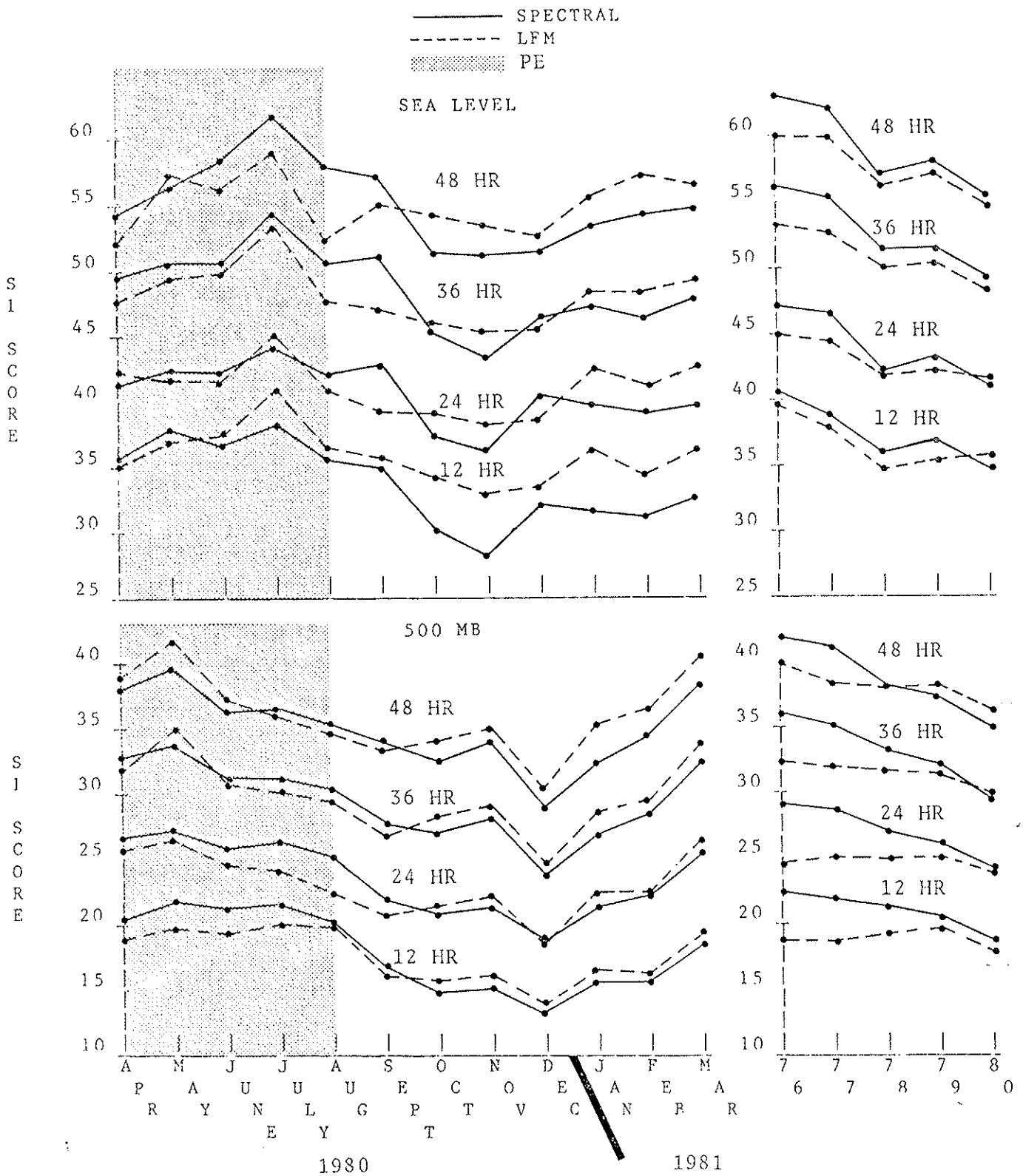

Figure 6

(Continued from inside front cover)

NWS 16 Storm Tide Frequencies on the South Carolina Coast. Vance A. Myers, June 1975, 79 p. (COM-75-11335)

NWS 17 Estimation of Hurricane Storm Surge in Apalachicola Bay, Florida. James E. Overland, June 1975. 66 p. (COM-75-11332)

NWS 18 Joint Probability Method of Tide Frequency Analysis Applied to Apalachicola Bay and St. George Sound, Florida. Francis P. Ho and Vance A. Myers, November 1975, 43 p. (PB-251123)

NWS 19 A Point Energy and Mass Balance Model of a Snow Cover. Eric A. Anderson, February 1976, 150 p. (PB-254653)

NWS 20 Precipitable Water Over the United States, Volume 1: Monthly Means. George A. Lott, November 1976, 173 p. (PB-264219)

NWS 20 Precipitable Water Over the United States, Volume II: Semimonthly Maxima. Francis P. Ho and John T. Riedel, July 1979, 359 p. (PB-300870)

NWS 21 Interduration Precipitation Relations for Storms - Southeast States. Ralph H. Frederick, March 1979, 66 p. (PB-297192)

NWS 22 The Nested Grid Model. Norman A. Phillips, April 1979, 89 p. (PB-299046)

NWS 23 Meteorological Criteria for Standard Project Hurricane and Probable Maximum Hurricane and Probable Maximum Hurricane Windfields, Gulf and East Coasts of the United States. Richard W. Schwerdt, Francis P. Ho, and Roger R. Watkins, September 1979, 348 p. (PB-80 117997)

NWS 24 A Methodology for Point-to-Area Rainfall Frequency Ratios. Vance A. Myers and Raymond M. Zehr, February 1980, 180 p. (PB80 180102)

NWS 25 Comparison of Generalized Estimates of Probable Maximum Precipitation With Greatest Observed Rainfalls. John T. Riedel and Louis C. Schreiner, March 1980, 75 p. (PB80 191463)

NWS 26 Frequency and Motion of Atlantic Tropical Cyclones. Charles J. Neumann and Michael J. Pryslak, March 1981, 64 p. (PB81 247256)

NWS 27 Interduration Precipitation Relations for Storms--Western United States. Ralph H. Frederick, John F. Miller, Francis P. Richards, and Richard W. Schwerdt, September 1981, 158 p.

NWS 28 GEM: A Statistical Weather Forecasting Procedure. Robert G. Miller, November 1981, 103 p.

NWS 29 Analyses of Elements of the Marine Environment for the Atlantic Remote Sensing Land Ocean Experiment (ARSLOE)--An Atlas for October 22 Through October 27, 1980. Lawrence D. Burroughs, May 1982, 116 p.

NOAA SCIENTIFIC AND TECHNICAL PUBLICATIONS

The National Oceanic and Atmospheric Administration was established as part of the Department of Commerce on October 3, 1970. The mission responsibilities of NOAA are to assess the socioeconomic impact of natural and technological changes in the environment and to monitor and predict the state of the solid Earth, the oceans and their living resources, the atmosphere, and the space environment of the Earth.

The major components of NOAA regularly produce various types of scientific and technical information in the following kinds of publications:

PROFESSIONAL PAPERS — Important definitive research results, major techniques, and special investigations.

CONTRACT AND GRANT REPORTS — Reports prepared by contractors or grantees under NOAA sponsorship.

ATLAS — Presentation of analyzed data generally in the form of maps showing distribution of rainfall, chemical and physical conditions of oceans and atmosphere, distribution of fishes and marine mammals, ionospheric conditions, etc.

TECHNICAL SERVICE PUBLICATIONS — Reports containing data, observations, instructions, etc. A partial listing includes data serials; prediction and outlook periodicals; technical manuals, training papers, planning reports, and information serials; and miscellaneous technical publications.

TECHNICAL REPORTS — Journal quality with extensive details, mathematical developments, or data listings.

TECHNICAL MEMORANDUMS — Reports of preliminary, partial, or negative research or technology results, interim instructions, and the like.

Information on availability of NOAA publications can be obtained from:

ENVIRONMENTAL SCIENCE INFORMATION CENTER (OA/D812)
ENVIRONMENTAL DATA AND INFORMATION SERVICE
NATIONAL OCEANIC AND ATMOSPHERIC ADMINISTRATION
U.S. DEPARTMENT OF COMMERCE

Rockville, MD 20852

NOAA--S/T 82-55